Journal of Solid State Chemistry **152,** 261–270 (2000)
doi:10.1006/jssc.2000.8691, available online at http://www.idealibrary.com on IDEAL®

Hydrogen Bond-Directed Hexagonal Frameworks Based on Coordinated 1,3,5-Benzenetricarboxylate

C. J. Kepert,[1] T. J. Prior,[2] and M. J. Rosseinsky[2,3]

Inorganic Chemistry Laboratory, Department of Chemistry, University of Oxford, South Parks Road, Oxford, OX1 3QR, U.K.

We report two phases containing the hexagonal (6,3) network of the graphene sheet derived by tridentate coordination of 1,3,5-benzenetricarboxylate to octahedral Ni^{II} centers. When the solvent used is 2-methyl-1-butanol, water directs the coordination about Ni^{II} and ABCA′B′C′ stacking of layers is obtained. The use of 1-butanol as solvent gives a different hydrogen-bonding arrangement around Ni^{II} and produces AAA stacking of the layers. We have previously demonstrated that the use of other alcohols such as methanol, ethanol, 1,2-ethanediol, and 1,2-propanediol leads to the formation of 3-D architectures. Here we show that a change in the hydrogen bonding around the metal center leads to 2-D structures which house substantial solvent-filled microcavities. The comparatively weak interactions between layers, and the relative importance of framework–solvent interactions, facilitates slippage of the hexagonal sheets and interconversion between stacking type with guest exchange.

***Key Words*: coordination polymer; network; framework solid; guest exchange; microcavity; interconversion; benzenetricarboxylate.**

INTRODUCTION

The new framework topologies (1) accessible from inorganic coordination polymers are attracting interest in an effort to replicate and extend the diverse sorption and catalysis chemistry of the aluminosilicates and their analogues (2). The stable open framework $Co(btc)_3(C_5H_5N)_2 \cdot \frac{2}{3}C_5H_5N$ is based on the 1,3,5-benzenetricarboxylate (btc) ligand coordinated to Co^{II} with pyridine as an axial spacer ligand and reversibly exchanges aromatic but not aliphatic guest molecules (3). Btc coordination frameworks incorporating hydrogen bonding and displaying selectivity to guest exchange have recently been reported (4). We recently reported the chiral porous coordination polymer $Ni_3(btc)_2(eg)_6(py)_6 \cdot 4H_2O \cdot 3eg$ (eg = 1,2-ethanediol, py = pyridine) which spontaneously resolves into homochiral single crystals and can resorb the cavity species liberated on heating without loss of crystallinity (5). Structurally similar materials are obtained from methanol and ethanol. In a search for optically active alcohols which will form this structure displaying quadruple interpenetration of the (10,3)-a network (6), we investigated the use of 2-methyl-1-butanol (mb) as a template. In contrast to ethanol and methanol, this alcohol leads to the formation of a two-dimensional network based on honeycomb layers ((6,3) nets), stacked ABCA′B′C′. The existence of a phase similar to this and unit cell parameters for it have already been reported (7), but here we present a full structural description. Similar hexagonal sheets are obtained when 1-butanol is used as the template, but the stacking sequence of the layers is now AAA. A similar stacking sequence in a btc framework has been reported recently by others (4b). In this paper we analyze how the difference between two- and three-dimensional frameworks with similar auxiliary ligand sets is controlled by the hydrogen bonding around the metal center.

EXPERIMENTAL

Synthesis

1-Butanol was obtained from BDH and all other reagents were obtained from the Aldrich Chemical Co. and used as supplied without further purification. For each alcohol, a 2-ml portion of an alcoholic solution containing a 3:2 stoichiometric mixture of $Ni(NO_3)_2 \cdot 6H_2O$ (0.0285 M) and H_3btc (0.019 M) was placed in a cylindrical 75- × 25-mm vial into which was placed a smaller vial containing 0.2 ml of pyridine (2.5 mmol) with a pierced stopper. The outer vial was sealed with parafilm and left to stand at room temperature for 2 weeks. For 2-methyl-1-butanol (mb) this method afforded deep blue cubic blocks (**1**) up to 0.5 mm in length and for 1-butanol light green-blue plates (**2**) up to $0.5 \times 0.3 \times 2\ mm^3$ were obtained.

[1] Current address: School of Chemistry, University of Sydney, NSW 2006, Australia.

[2] Current address: Department of Chemistry, University of Liverpool, Liverpool, L69 7ZD, U.K.

[3] To whom correspondence should be addressed. E-mail: m.j.rosseinsky@liv.ac.uk.

0022-4596/00 $35.00

Structure Determination

Single-crystal X-ray diffraction data were recorded on an Enraf-Nonius DIP2000 image plate diffractometer with Mo$K\alpha$ radiation at 150 K. Crystals were quench cooled in the nitrogen gas cryostream. Ninety images were recorded employing successive 2° rotations in ϕ and reduced with the HKL suite of programs (8). Structure solution was carried out using SHELXS-86 (9). A summary of crystallographic information and refinement details is given in Table 1. Full-matrix least-squares refinement of the structure was carried out within SHELXL-93 (10). For **1** many of the framework hydrogen atoms were located by difference Fourier methods; other hydrogens were placed by geometric considerations. Two mb molecules in the asymmetric unit are heavily disordered, one being disordered about a three-fold rotation axis. For **2** hydrogen atoms were placed using geometric criteria. There is extreme disorder in the carbon atom positions of both the coordinated and noncoordinated 1-butanol molecules. These units were modeled in many cases as split over two or more orientations. For most of these species it was not possible to locate the outer carbon atoms. Of the $Ni_3(btc)_2$ framework atoms, only those in the direct neighborhood of Ni4 (which was refined isotropically with 50% occupation and lies 0.30 Å from an inversion center) were modeled as disordered. A second site for Ni4, lying 1.07 Å from the inversion center, refined with an occupation of 0.037.

Thermogravimetric Analyses

These were performed on a Rheometric Scientific STA 1500 instrument in order to study the loss of interlayer species as a function of time and temperature. Samples were heated under flowing nitrogen to 600°C ramped at 2°C min^{-1}.

Powder X-Ray Diffraction

Powder X-ray data were recorded on a Siemens D5000 diffractometer operating in transmission geometry with samples mounted in 0.5-mm glass capillaries, Cu$K\alpha_1$ radiation from a Ge monochromator, and a 6° linear position-sensitive detector. Reabsorption studies were carried out by allowing open capillaries to equilibrate with pyridine vapor in closed containers. Reabsorption is not seen when samples are left to stand in air, ruling out the possibility that water is responsible for the observed return of crystallinity.

Vibrational Spectroscopy

Infrared data were collected on samples prepared as KBr disks in an airtight cell over the range 400–4000 cm^{-1} using a Mattson Instruments Galaxy Series FTIR 6020 spectrometer. Desolvated samples were stored under dry N_2 between preparation and measurement, and all KBr disks were also handled under this inert atmosphere.

TABLE 1
Structural Details from Single-Crystal and Powder X-Ray Diffraction of 1, 2, and the Pyridine-Resolvated Forms of Their Desolvates

Compound/solvent	2-Methyl-1-butanol (**1**)	2-Methyl-1-butanol (**2**)	Butanol	Py-resolv of **1**	Py-resolv of **2**
Formula	$C_{181}H_{225}N_{21}Ni_6O_{38}$	—	$C_{88}H_{136}N_6Ni_3O_{22}$	—	—
FW/g mol^{-1}	3655.08	—	1806.16	—	—
T/K	150(2)	293(2)	150(2)	293(2)	293(2)
Method	Single crystal	Powder	Single crystal	Powder	Powder
λ/Å	0.71073	1.54056	0.71073	1.54056	1.54056
Color	Blue	Blue	Blue	Bluish-purple	Deep blue
Size/mm^3	$0.40 \times 0.35 \times 0.30$	—	$0.38 \times 0.16 \times 0.12$	—	—
Crystal system	Trigonal	Trigonal	Triclinic	Trigonal	Trigonal
Space group	$R\bar{3}$ (No. 148)	—	$P\bar{1}$ (No. 2)	—	—
a/Å	19.546(1)	19.713(3)	9.097(1)	19.674(5)	19.501(1)
b/Å	19.546(1)	19.713(3)	16.661(1)	19.674(5)	19.501(1)
c/Å	42.028(1)	43.02(2)	32.591(2)	43.03(3)	42.504(6)
α/°	90	90	91.017(5)	90	90
β/°	90	90	89.957(4)	90	90
γ/°	120	120	86.471(4)	120	120
V/Å^3	13905.5(11)	14478(7)	4929.5(7)	14424(11)	13998(2)
Z	3	—	2	—	—
ρ_{calc}/Mg m^{-3}	1.309	—	1.217	—	—
μ/mm^{-1}	0.675	—	0.635	—	—
$2\theta_{max}$/°	52.92	—	48.22	—	—
Data/restraints/parameters	6368/177/408	—	14716/1618/905	—	—
$R(F)$/% $\{I > 2\sigma(I)$, all data$\}$	0.0910 {0.0991}	—	0.0859 {0.1400}	—	—
$R_w(F^2)$/% $\{I > 2\sigma(I)$, all data$\}$	0.2304 {0.2337}	—	0.2442 {0.2765}	—	—
GOF	1.159	—	0.995	—	—

RESULTS

Both of the phases reported here display the (6,3) net of the graphene sheet. In both compounds the hexagonal rings are constructed from six btc anions which act as tridentate, triangular connectors, linearly bridged by octahedrally coordinated Ni^{II} cations.

1 crystallizes in the centrosymmetric space group $R\bar{3}$ (see Table 1 for crystallographic details). Chemical analysis of **1** is approximately consistent with the composition predicted crystallographically: for $Ni_3(btc)_2(py)_9(H_2O)_3 \cdot 3.3(C_5H_{12}O) \cdot 1.5(py) \cdot 4(H_2O)$, calculated % C 56.85, H 6.16, N 8.00, Ni 9.58; found % C 56.89, H 6.18, N 8.01, Ni 9.54. The volatility of the cavity species obviously leads to a significant uncertainty in the exact composition. Analysis of the micropores using PLATON (11) indicates that 31.6% of the crystal volume is taken up with unbound solvent. **1** exhibits a nearly planar (6,3) net made of hexagons of side 11.285(1) Å in length at 150 K, comprised of six btc anions linked by octahedral nickel cations, shown in Fig. 1. As in the three-dimensional structures adopting the (10,3)-a net, the carboxylate groups of the btc ligand occupy *trans* positions in the coordination sphere of the nickel. Successive layers have a mean separation of 7.005 Å. The *R*-centering translations and the inversion centers located between the layers give an ABCA′B′C′ stacking sequence which places the voids in the centers of the rings in one layer juxtaposed with btc anions in adjacent layers thus removing the possibility of channels parallel to the stacking direction. Layers designated A and A′ are arranged such that the centers of hexagons are aligned. However, as these layers are chemically distinct they are not related by a translation of $c/2$. This stacking arrangement is shown in Fig. 2.

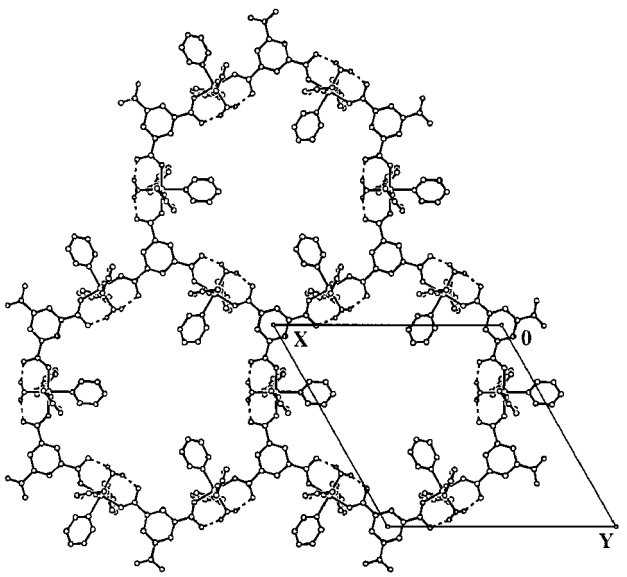

FIG. 1. Hexagonal Ni_3btc_2 sheets in **1** viewed along the stacking direction with the solvent in the cavities omitted for clarity. The pores within the layers are defined by the van der Waals surfaces of the coordinated pyridine molecules projecting into the pores as equilateral triangular in shape with side 5.03 Å.

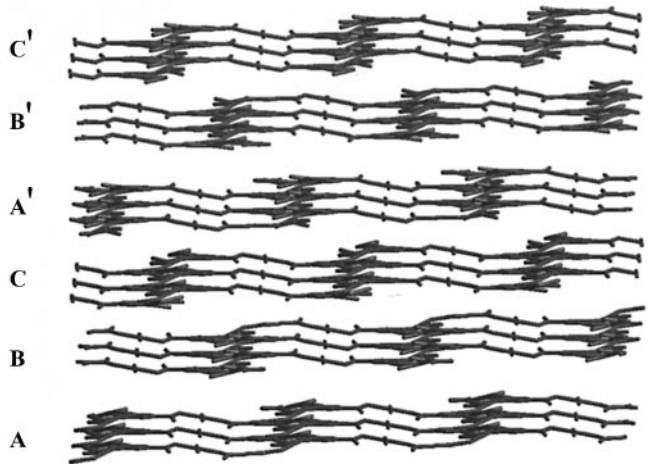

FIG. 2. Rhombohedral stacking of the hexagonal Ni_3btc_2 sheets in **1** yields an ABCA′B′C′ layer sequence in which btc centroids from adjacent layers obstruct the centroids of the layer pores, preventing the formation of linear channels. Only the Ni and btc units are represented for clarity.

In contrast to the behavior for methanol, ethanol, and 1,2-ethanediol, the mb does not bind to the metal center, which is considered a consequence of its significant steric bulk. The coordination sphere of the nickel is completed by three pyridines and one water molecule, as shown in Fig. 3. The oxygen atom of this water molecule refined as being 84 : 16 disordered over two sites separated by 0.49 Å, each site participating in two hydrogen bonds to the free oxygen atoms of the carboxylate groups. The nonplanarity of the $Ni–OH_2$ unit induces a slight puckering of the hexagonal sheet through the influence of this water–carboxylate hydrogen bonding (see Figs. 2 and 3). This puckering results in the benzene rings lying displaced from the layer defined by the nickel atoms by 0.33 Å. The layer puckering has interesting influences on the layer packing and also on the chemical environments of alternating interlayer microcavities. There are a large number of weak interlayer CH(pyridine)$\cdots$O(carboxylate) hydrogen-bonding interactions which control the interlayer separation distances, which alternate at 6.721 and 7.288 Å (for planes defined by Ni atoms; a full analysis of layer–layer interactions is available from the authors). Notably, the noncoordinated oxygen atoms of the framework carboxylate groups project slightly into every second interlayer as a result of the puckering. Highly disordered mb and pyridine lie between the layers as shown in Fig. 4. The stacking of puckered layers results in a striking differentiation between the pyridine and mb guests located between the layers. Pyridine is found only in alternate interlayer voids and is located such that the centroid of the

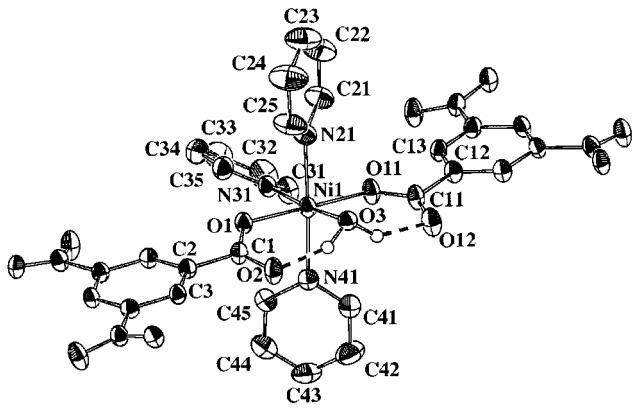

FIG. 3. ORTEP representation (50% ellipsoids) of the asymmetric unit of **1** (framework only). The dashed lines represent hydrogen bonding between the water and the carboxylate group.

pyridine ring lies directly between two symmetry-equivalent hydrogen atoms of a bound pyridine in each layer (Fig. 5a) The distance (C–H $\cdots \pi$) from pyridine centroid to hydrogen atom is 2.73 Å, which is in good agreement with published values for similar systems (12). Each hydrogen is located so that a vector joining it to the centroid of the pyridine ring is normal to the plane of the ring and the C–H $\cdots$ centroid angle is 147.4°. In voids where pyridine is not found the equivalent distance from the midpoint between the layers to the H atom is 2.38 Å. It seems therefore that this interaction is strongly dependent on the size of the cavity produced by the C–H bonds from the pyridine molecules in neighboring layers. In the corresponding cavities of the alternate interlayers, mb is found in place of pyridine (Fig. 5b) This mb molecule hydrogen bonds to the framework via the nonbonding oxygen atom of the btc carboxylate, with an O $\cdots$ O distance of 2.862(14) Å. The presence of mb in this void rather than pyridine may be attributed to the favorable

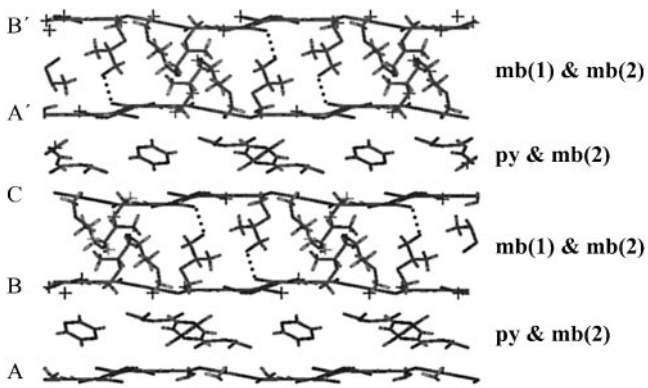

FIG. 4. Distribution of pyridine (py) and 2-methyl-1-butanol (mb) between layers in **1**. Pyridine is found only in alternate interlayer spaces, together with mb(2) which is located in all the interlayer regions. mb(1) occupies the interlayers which do not contain pyridine.

orientation of the carboxyl groups for hydrogen bond formation, caused by the slight puckering of the M_3btc_2 layer.

A second mb molecule lies on the *z*-axis and is disordered about a three-fold axis and modeled as occupying each of the three possible orientations equally. The mb molecule lies directly above the centroid of the aromatic ring of a btc, so that the proton is approximately 3 Å from it. The C–H $\cdots$ centroid angle is 180°, while a vector joining the centroid of the ring and the proton is normal to the plane of the ring as they interact with the btc anions which are essentially parallel to the layer rather than the tilted bound pyridine molecules projecting into the interlayer space.

Analysis of the micropore volumes suggests there are two other cavity regions capable of housing solvent molecules, each one defined by a hexagon of six pyridine ligands projecting between the layers. These are centered on $(0, 0, 0)$ and $(0, 0, \frac{1}{2})$, have respective volumes of 66 and 85 $Å^3$, and lie 3.95 and 4.11 Å away from their nearest contacts on the pyridine molecules. It is suspected that a highly disordered water molecule occupies each of these cavities: modeling of the diffuse electron density observed in these regions with partially occupied oxygen atoms gave highly unstable refinements and so these regions were left empty in the structural model.

2 adopts the centrosymmetric space group $P\bar{1}$ (see Table 1 for crystallographic details). Chemical analysis of **2** is approximately consistent with the composition obtained from the crystal structure, but the volatility of the interlayer species obviously introduces errors. For $Ni_3(btc)_2(py)_6$ $(^nBuOH)_6 \cdot 2.2(^nBuOH) \cdot 6.5(H_2O)$, calculated % C 54.21, H 7.39, N 4.69, Ni 9.83; found % C 54.23, H 7.09, N, 4.86, Ni 9.72. The volume occupied by unbound solvent was found to be 33%. **2** displays a rumpled (6,3) net, formed from hexagons of side 11.238(1) Å, which is severely puckered away from ideal geometry as shown in Fig. 6. The angle subtended by the planes of adjacent hexagons is 142.8°, in contrast to **1** for which the mean planes of the hexagons are coplanar. These hexagonal sheets are stacked in AAA fashion so that the voids at the centers of the hexagonal rings are aligned in adjacent layers and lie a mean distance of 9.097(1) Å apart (Fig. 7; a complete analysis of interlayer hydrogen-bonding interactions is available from the authors). The channels parallel to the crystallographic *x*-axis are flattened cylindrical in shape with dimensions 13.7×13.4 $Å^2$ (defined as atom-to-atom distances) and are filled with 1-butanol. Further work in an attempt to join adjacent layers by judicious choice of equatorial ligands coordinated to the metal is currently underway.

In a similar fashion to **1**, the six-membered rings are made up of six btc anions joined by nickel cations acting as linear connectors, but the remaining coordination sites on nickel are completed in a markedly different way. Figure 8 shows the four equatorial sites occupied by two pyridine and two

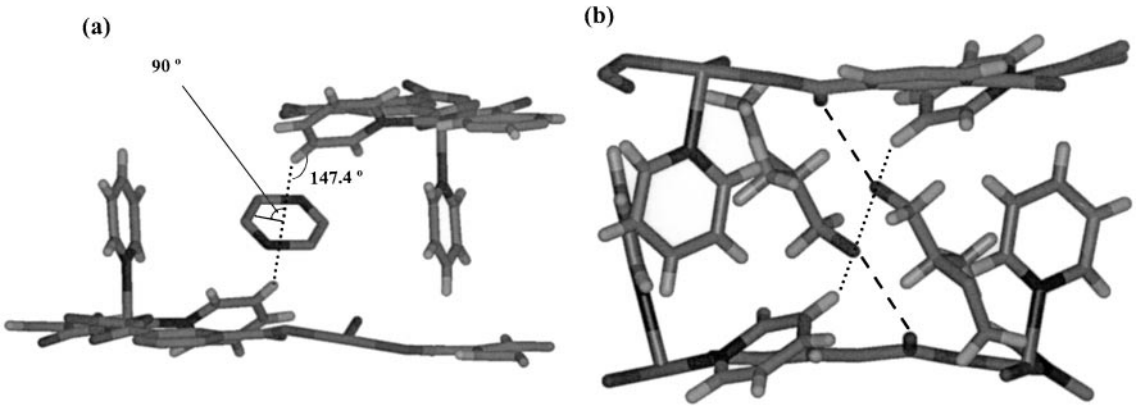

FIG. 5. Location in **1** of (a) pyridine bound by C–H $\cdots \pi$ interactions (dotted lines) to coordinated pyridine ligands between the Ni_3btc_2 sheets and (b) 2-methyl-1-butanol bound via hydrogen bonds (dashed lines) to the carboxylate anions in the Ni_3btc_2 sheets.

1-butanol molecules in a *trans* arrangement. In contrast to mb, the more hydrophilic and less bulky 1-butanol molecules act as a ligand to Ni^{II} but are arranged *trans* rather than *cis* at the metal center. The alkyl chains of these molecules extend toward the centers of the hexagonal rings into the channels, where they may "wag" freely with large thermal motion and are therefore modeled by multiple orientations (Fig. 8).

The presence of two alcohol and two pyridine ligands coordinated to the metal is also observed for the 3-D architectures containing the (10,3)-a net previously obtained (5). However, here the alcohol ligands are arranged in a *trans* fashion, while they are *cis* when 3-D frameworks result. It is the resulting hydrogen bonding between the alcohol ligands and the two carboxylate units that determines the structure obtained. The Discussion section contains further coverage of this point. The asymmetric unit is uncommonly large, having over 120 independent nonhydrogen atoms and there is a significant amount of disorder in the framework. One of the four independent nickel cations, Ni(4), has 50% occupation and lies displaced 0.30 Å from an inversion center. Consequently, the ligands bound to this cation are also modeled over two sites. In between the layers lies highly disordered solvent. Three separate unbound molecules of 1-butanol were located in the asymmetric unit, all of which hydrogen bond to the framework through the nonbonding carboxylate oxygen atom. Two of these molecules are well resolved crystallographically: one binds tightly to the framework (O $\cdots$ O 2.73(6) Å) and the second is less strongly bound (O $\cdots$ O 2.98(3) Å). The third molecule is poorly resolved and appears to be bound to the framework at a greater distance. The alkyl chains of the interlayer solvent are highly disordered and modeled over a number of atomic positions.

For coordination polymers derived from multidentate carboxylates, where auxiliary ligands possess hydrogen-bonding capability (e.g., alcohols, amines), it appears that interligand hydrogen bonding about a metal cation is crucial in determining the carboxylate orientation and hence the structure obtained (5). The example of **1** and **2** illustrates this theme. The hydrogen bonding of the ligands about Ni^{II} in **1** and **2** is shown in Fig. 9. For **1** the water bridges both of the nonbonding oxygen atoms of the carboxylates and locks them in the same plane. The O(3) $\cdots$ O(carboxylate) distan-

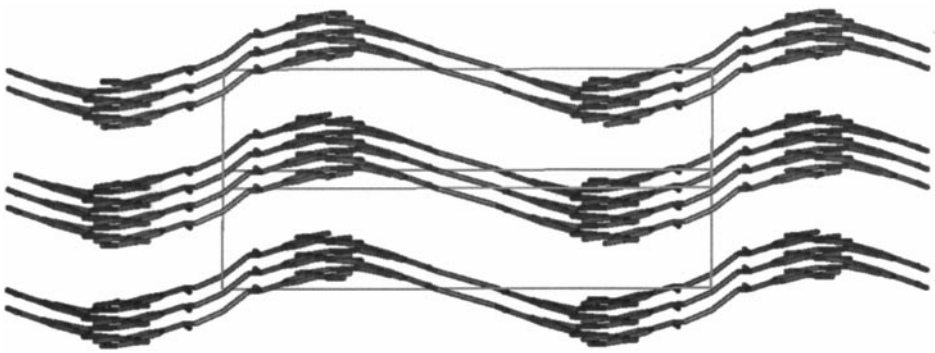

FIG. 6. Severely puckered Ni_3btc_2 sheets of **2** viewed approximately perpendicular to the stacking direction of the AAA sequence.

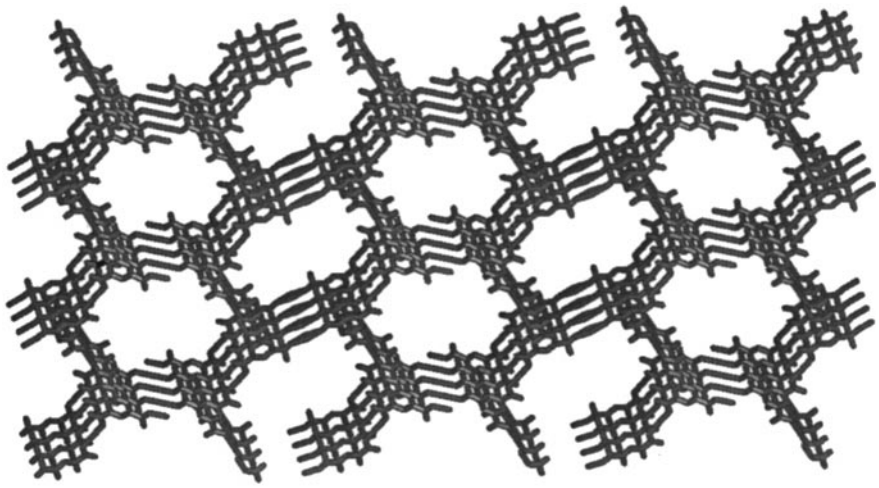

FIG. 7. View along *a* showing the channels in **2** formed by the AAA layer stacking.

ces for this interaction, 2.602(6) and 2.696(7) Å for O(2) and O(12), respectively, are within expected hydrogen bond distances. The longer O(3) ··· O(12) distance reflects a weakening of this interaction due to the presence of the O(12) ··· mb(solvent) hydrogen bond. For phase **2** the oxygen atom of the alcohol can only hydrogen bond to one carboxylate; the six independent O ··· O distances range from 2.543(8) to 2.581(9) Å. Furthermore, the *trans* arrangement of the 1-butanol molecules locks the nonbonding oxygen atoms of the carboxylates on opposite sides of the cation. The influence of this hydrogen-bonding is seen in the infrared absorption spectra for **1** and **2.** Where the nonbonding oxygen of a carboxylate is involved in a hydrogen-bonding interaction such as that observed here ("pseudobridging") (13) the splitting between symmetric and antisymmetric carboxylate stretches, Δ, is less than the value for the ionic carboxylate. The value of Δ for the btc anion (potassium salt) is 201(1) cm^{-1}. For **1** the antisymmetric stretch is split into two bands at 1542(1) cm^{-1} and a weaker band at 1577(1) cm^{-1}. The predominant asymmetric stretch gives $\Delta = 169\ cm^{-1}$, which is consistent with the pseudobridging behavior observed in the crystal structure. The weaker band yields $\Delta = 204\ cm^{-1}$ which confirms that solvent and water ligands are lost from **1** during preparation of the KBr disk under dry N_2 as it is obvious that some of the carboxylate is not involved in hydrogen bonding. **2** similarly displays two asymmetric stretch bands: one at 1544(1) cm^{-1} and a weaker band at 1562(1) cm^{-1}. Δ here is 174(1) cm^{-1} for the stronger band, agreeing with the pseudobridging hydrogen bonding observed crystallographically, and 193 cm^{-1} for the other band, suggesting that some of the 1-butanol ligands have been lost during preparation.

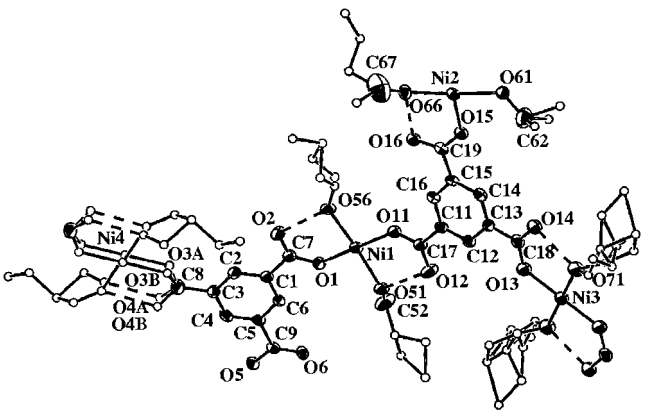

FIG. 8. ORTEP of part of the asymmetric unit of **2** (30% ellipsoid for anisotropic atoms).

The thermal behavior of the phases **1** and **2** is remarkably similar as shown in Fig. 10. Both phases lose solvent when allowed to stand in air, which is accompanied by a whitening of the crystal surface. Heating phase **1** to 75°C results in a slight loss of mass (2.5%). Above this temperature there is a prominent step in the TGA, 40.9% of the original mass, which is due to loss of much of the interlayer solvent and some of the equatorial ligands bound to the metal. For phase **1** heating to 150°C produces a phase shown by chemical analysis to be $Ni_3(btc)_2(py)_{5.3}(H_2O)_3 \cdot 1.8(C_5H_{12}O) \cdot 4(H_2O)$ (calcd % C 48.92, H 5.13, N 5.85, Ni 13.87; found % C 48.88, H 4.66, N 5.82, Ni 13.65.) The estimate of the amount of retained water in the desolvated phase found by analysis is undoubtedly an overestimate due to the rapid resorption of water by the intermediate. For this material IR spectroscopy shows that the antisymmetric carboxylate stretch is split into two bands of approximately equal intensity at 1546(1) and 1572(1) cm^{-1}. Δ is

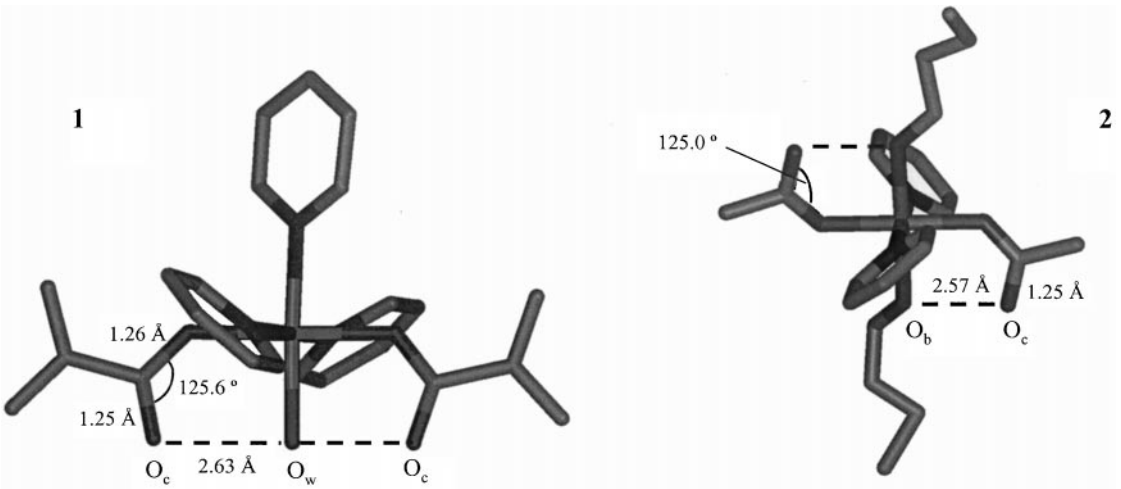

FIG. 9. In **1**, water acts as a double H-bond donor producing a 180° arrangement of the carboxylates around the metal resulting in flat Ni_3btc_2 sheets. Hydrogen bonds between the oxygen atoms of the water (O_w) and carboxylate (O_c) are shown as dashed lines. In **2** each of the *trans*-1-butanol molecules is only able to donate a single proton thereby modifying the orientation of the *trans* carboxylate groups. Hydrogen bonds between oxygen atoms of butanol (O_b) and the carboxylate (O_c) are shown as dashed lines.

therefore 199 and 173 cm^{-1} which is suggestive of two different modes of carboxylate coordination within this phase, i.e., unidentate to the metal without and with hydrogen bonding to neighboring H-bond donors, respectively. Powder X-ray diffraction shows this desolvated phase to be amorphous.

Heating phase **2** to 70°C results in a loss of mass of 3.7%, but above this there is a sharp mass loss of 42.3% upon heating to 150°C. This generates a phase with composition from chemical analysis $Ni_3btc_2(py)_{4.4}(C_4H_{10}O)_{0.6}\cdot 6.4(H_2O)$ (calcd % C 46.61, H 4.43, N 5.55, Ni 15.82; found % C 46.49, H 4.38, N 5.55, Ni 15.75). This corresponds to loss of all of the interlayer 1-butanol and approximately half of the equatorial ligands and is in tolerable agreement with the observed mass loss (calcd mass loss 38.6%). Powder X-ray diffraction shows this material to be amorphous. This desolvated phase also displays splitting in the asymmetric carboxylate stretch, with two equally intense bands at 1549(1) and 1572(1) cm^{-1}, suggesting two different carboxylate coordination geometries as for phase **1**. Δ is 199 and 176 cm^{-1}, which is consistent with some of the carboxylate being unidentate and some being "pseudobridged"

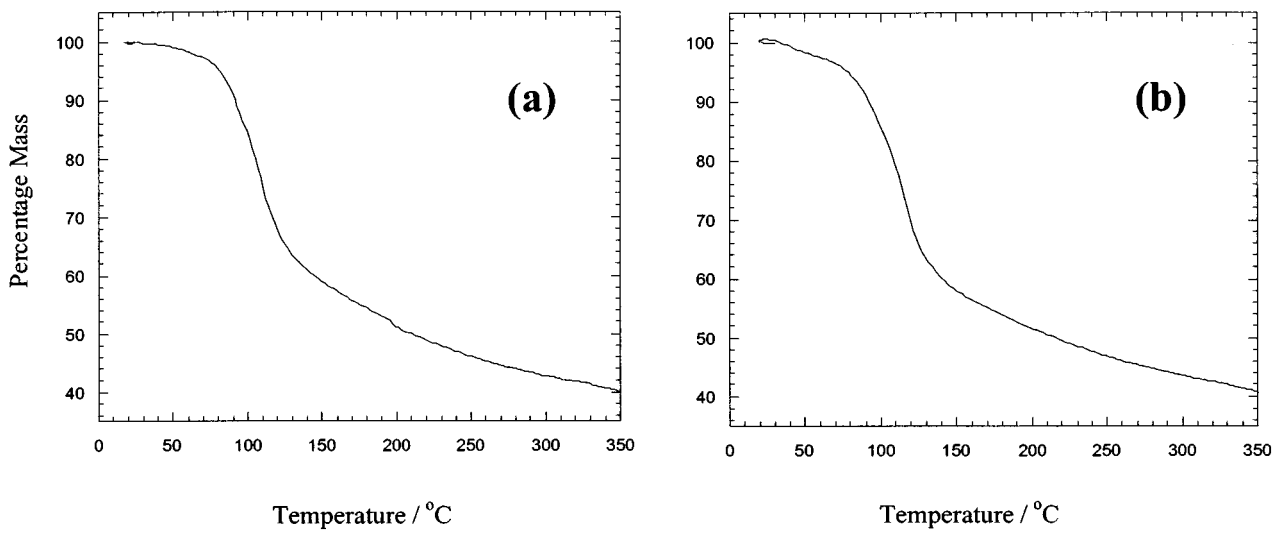

FIG. 10. Thermogravimetric analysis of **1** (a) and **2** (b) under flowing nitrogen.

to 1-butanol or water via hydrogen bonds. It appears therefore that heating to 150°C removes all of the interlayer 1-butanol, but the coordination requirement of Ni^{II} is satisfied by pyridine, some 1-butanol, and water. For neither desolvated phase **1** nor **2** is there spectroscopic evidence that the amorphous intermediate contains bidentate btc coordination, which would be shown by a very small value of Δ compared with that for the free anion. This suggests that each desolvated phase contains vacant coordination sites which could be readily filled if the material was exposed to suitable ligand, such as water or pyridine.

Resorption of Pyridine by Desolvated 1 and 2

Exposure of the desolvated form of phase **1** to pyridine vapor leads to a dramatic increase in crystallinity as shown in Fig. 11a. After 1 day of exposure pyridine vapor, samples at the top of capillaries that had been exposed to pyridine changed color from light blue to bluish-purple. Features are visible in the powder diffraction pattern consistent with return of the original structure. After 11 days the material is highly crystalline and has unit cell parameters $a = 19.674(5)$ Å and $c = 43.03(3)$ Å (Table 1). These values are strikingly similar to the values for phase **1** at room temperature; in particular, the average interlayer separation is the same within error, although a slight contraction in the xy plane has occurred.

Exposure of the desolvated form of phase **2** to pyridine vapor leads to a marked increase in crystallinity as shown in Fig. 11b. The features which are present in the powder X-ray diffraction pattern after 4 days of exposure to pyridine vapor are similar to those of the phase **1**. Upon further exposure to pyridine a highly crystalline material which can be indexed on a trigonal cell with parameters $a = 19.501(1)$ Å, $c = 42.504(6)$ Å (Table 1) is obtained. At no point during this resorption of pyridine is the pattern due to the phase **2** returned; this interconversion occurs without regeneration of the original starting material.

DISCUSSION

The btc ligand is extremely versatile in the formation of coordination polymer networks with both transition (2) and main group (14) metals. The most obvious distinction between the nets formed is their dimensionality, and this study reveals the key features within the coordination sphere of the metal differentiating between 3-D frameworks and the 2-D layered structures found here.

For the alcohols methanol, ethanol, and 1,2-ethanediol 3-D architectures are obtained with two *cis* unidentate alcohol ligands at the octahedral metal center (5). These hydrogen bond to the carboxylate groups which are therefore approximately perpendicular. In the case of 1,2-ethanediol the angle between the btc planes is the tetrahedral angle. This arrangement of triangular connectors with a 109° 26′ rotation gives rise to an undistorted (10,3)-a network. In the present hexagonal phases, the hydrogen bond donors interacting with the carboxylate are not located *cis* (perpendicular) to each other, which enforces the 2-D motif. In **1** the btc planes are locked approximately planar by the presence of one bridging water molecule.

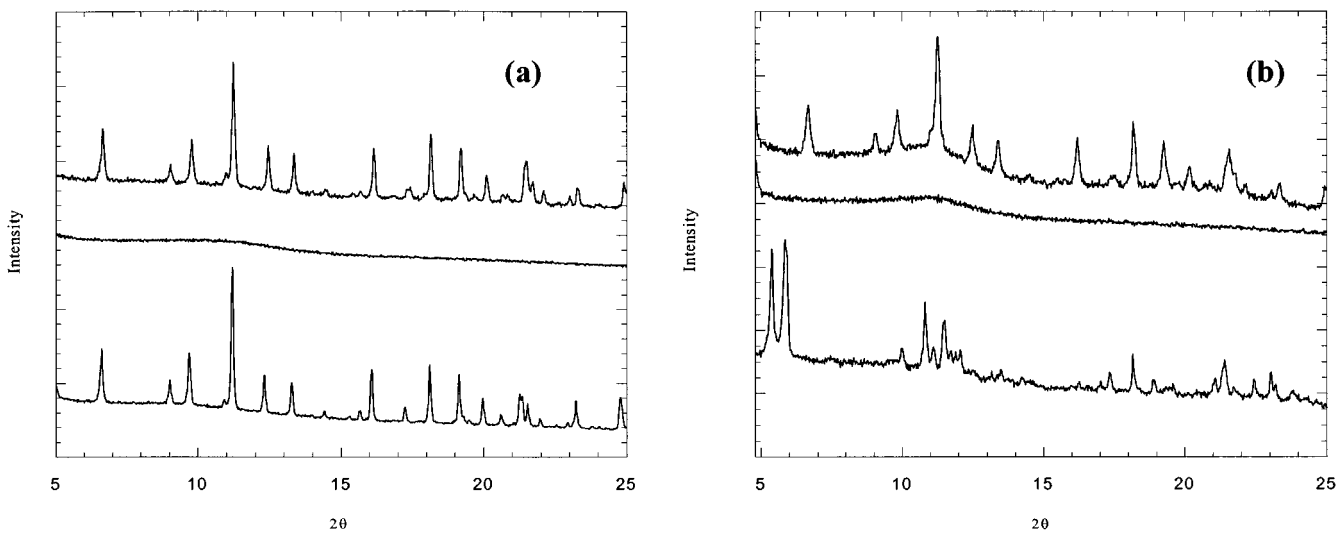

FIG. 11. (a) X-ray powder diffraction shows that crystalline **1** (lower line) may be desolvated to 150°C (coincident with the weight loss in Fig. 10a) to yield an amorphous phase (middle line). Exposure to pyridine vapor regenerates the ABC layer stacking of **1** (upper line). (b) Desolvation of crystalline **2** (lower line) produces an amorphous intermediate (middle line) which sorbs pyridine to give a rhombohedral phase with the ABCA′B′C′ stacking of **1**.

Similarly in **2** *trans* hydrogen-bonding alcohol ligands lock the btc units in approximately the same plane.

The existence of essentially planar layers in **1** having parallel btc planes compared to the highly rumpled layers of **2**, where the angle between btc planes is 148.15° for btc's linked by Ni(1) and Ni(2) and 0° for those linked by Ni(3) and Ni(4), seems likely to stem from a maximization of interlayer and layer–solvent van der Waals interactions rather than from any steric influence arising from the metal atom coordination. It is noted that highly efficient arrays of interlayer pyridine … carboxylate hydrogen-bonding interactions are achieved in both cases despite the different stacking types. The rumpling of layers in **2** appears to be necessary to achieve the observed extent of interlayer hydrogen bonding in the AAA stacking type.

The difference in species found within alternate interlayer voids is an intriguing feature of the structure of **1**. The reasoning for the different environments in these regions is quite subtle and is correlated to the alternating orientations of the coordinated water molecules in neighboring layers. In each hexagonal ring composed of six btc anions joined by Ni^{II}, alternate btc units lie at z-coordinates which differ slightly so that there are three btc anions at $z = n/6 + 0.074$ and three at $z = n/6 + 0.090$ (n is an integer). This equates to a height difference of 0.672(1) Å. The equatorial ligands around the octahedral Ni^{II} connectors joining the btc anions are therefore tilted away from the mean plane of the ring. The effect of this tilting is to push the pyridine ligand which lies *trans* to the water slightly above the mean plane of the ring. This is mirrored in the next layer up where the pyridine is tilted slightly down. This alternating pattern of up and down tilting of the in-layer pyridine leads to successive interlayer regions having alternating long and short C–H ⋯ H–C distances (Fig. 12) Between layers where this distance is longer (5.46 Å) pyridine is bound by the C–H ⋯ π interaction to the ligands which tilt into the interlayer void (Fig. 5a). Where this distance is shorter (4.76 Å) then pyridine is not bound (Fig. 5b) and mb is located around this site instead.

The loss of the guests between the layers above 150°C leads to a loss of crystallinity but IR spectroscopy shows that the bonding within the layers is essentially similar in the amorphous and crystalline solvated states. This is consistent with the ready regeneration of the layered structure **1** upon resolvation of desolvated intermediates from both phases. The main response of the btc is the loss of hydrogen bonding to other ligands in the metal coordination sphere rather than bidentate coordination to the metal as might be expected. The IR spectra show that the btc anion never becomes bidentate to the metal, the only differences being whether or not H-bonding to neighboring solvent is possible. This means that the desolvation also produces vacant coordination sites at the metal.

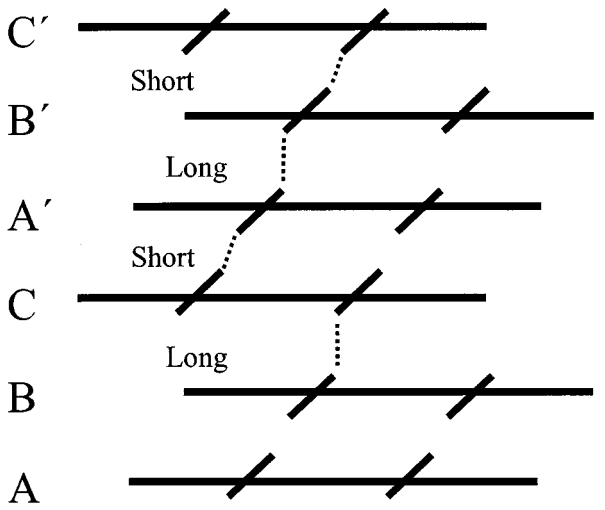

FIG. 12. Origin of the alternation in the guest species located between alternate layers in **1** is the tilting of pyridine ligands bound to the metal away from the mean planes of the layers. Pyridine molecules are located between layers where there are long C–H ⋯ H–C contacts, which create favorable cavities for C–H ⋯ π interactions.

These vacant sites allow the resolvating pyridine ligand to direct the course of the resolvation toward the trigonal ABC layer stacking of phase **1**, which contains three pyridine ligands in the first coordination sphere of the metal. This structure may also be favored in the presence of excess pyridine due to the specific solvation of this molecule between alternate layers. The interlayer solvent appears crucial for maintaining the registry of the layers and hence the crystallinity of both stacking sequences.

CONCLUSIONS

The hydrogen bonding to auxiliary ligands connected to the metal controls the dimensionality of coordinated btc frameworks. The composition of the first coordination sphere of the metal is itself controlled by the steric bulk of the ligands, with the secondary alcohol 2-methyl-1-butanol being excluded from the coordination sphere in preference to water, which is found only as a cavity species in frameworks formed by 1,2-ethanediol and ethanol. The 2-D structures are both based on the same (6,3) net whose stacking sequence controls the location of the interlayer guests. The ABC sequence of **1** appears particularly favorable for the location of pyridine by C–H ⋯ π interactions, and this stacking sequence is generated from the AAA sequence of **2** on loss of solvent followed by resolvation with pyridine. The intrinsic 2-D nature of the structure limits its robustness to guest loss, as the registry between the layers appears controlled by interactions with the guests. The generation of rigid structures based on these 2-D arrays will require stronger covalent or hydrogen bond linkages between the metal centers.

ACKNOWLEDGMENTS

C.J.K. thanks Christ Church, Oxford, for a Junior Research Fellowship. We thank EPSRC for a studentship to T.J.P. and funding of the single-crystal diffractometers used in this work, Dr. G. S. McGrady for assistance with IR spectroscopy, and Professor C. K. Prout and Dr. D. J. Watkin for useful discussions concerning crystallography.

REFERENCES

1. (a) B. F. Hoskins and R. Robson, *J. Am. Chem. Soc.* **112,** 1546 (1990); (b) S. R. Batten and R. Robson, *Angew. Chem., Int. Ed. Engl.* **37,** 1461 (1998); (c) B. F. Abrahams, S. R. Batten, M. J. Grannas, H. Hamit, B. F. Hoskins, and R. Robson, *Angew. Chem., Int. Ed. Engl.* **38,** 1475 (1999).
2. O. M. Yaghi, H. L. Li, C. Davis, D. Richardson, and T. L. Groy, *Acc. Chem. Res.* **31,** 474 (1998).
3. O. M. Yaghi, G. M. Li, and H. L. Li, *Nature* **378,** 703–706 (1995).
4. (a) O. M. Yaghi, H. L. Li, and T. L. Groy, *Am. Chem. Soc.* **118,** 9096–9101 (1996); (b) H. J. Choi and M. P. Suh, *J. Am. Chem. Soc.* **120,** 10622 (1998).
5. C. J. Kepert and M. J. Rosseinsky, *Chem. Commun.* 31–32 (1998).
6. A. F. Wells, "Three-Dimensional Nets and Polyhedra." Wiley-Interscience, New York, 1977.
7. S. S.-Y. Chui, S. M.-F. Lo, J. P. H. Charmant, A. G. Orpen, and I. D. Williams, *Science* **283,** 1148–1150 (1999).
8. Z. Otwinowski and W. Minor, *in* "Processing of X-ray Diffraction Data Collected in Oscillation Mode" (Z. Otwinowski and W. Minor, Eds.) pp. 276. Academic Press, New York, 1996.
9. G. M. Sheldrick, SHELXS-86, Universität Gottingen, 1986.
10. G. M. Sheldrick, SHELXL-93 Program for the refinement of crystal structures, Universität Gottingen, 1993.
11. A. L. Spek, *Acta Crystallogr. Sect. A* **46,** 194 (1990).
12. T. Steiner, *J. Chem. Soc., Chem. Commun.* 95 (1995).
13. G. B. Deacon and R. J. Phillips, *Coord. Chem. Rev.* **33,** 227 (1980).
14. M. J. Plater, A. J. Roberts, and R. A. Howie, *Chem. Commun.* 893 (1997).